Zeolitic Imidazolate Framework Cores Decorated with Pd Nanoparticles and Coated Further with Metal-Organic Framework Shells (ZIF-8@Pd@MOF-74) as Nanocatalysts for Chemo-Selective Hydrogenation Reactions

Changyan Guo[a], Caihong Liang[b], Xueping Qin[b], Yanjuan Gu[a], Ping Gao[b], Minhua Shao[b]*, Wing-tak Wong[a]*

[a] Department of Applied Biology and Chemical Technology, The Hong Kong Polytechnic University, Hong Kong Special Administrative Region, PR China.

[b] Department of Chemical and Biological Engineering, The Hong Kong University of Science and Technology, Hong Kong Special Administrative Region, PR China.

Abstract: The selective hydrogenation of Ar-C=C in the presence of Ar-NO_2 is a long-standing challenge because of the uncontrolled non-selective nature of hydrogenation. In this study, core-shell nanocatalyst ZIF-8@Pd@MOF-74 is developed for the preferential reduction of the Ar-C=C group. The ZIF-8 core can act as an effective support for Pd nanoparticles (NPs), and MOF-74 shell can prevent Pd NPs from leaching and oxidation. Compared with Pd/C and ZIF-8@Pd catalysts, our ZIF-8@Pd@MOF-74 nanocatalyst shows enhanced activity and selectivity for conversion of nitrostyrene to 1-ethyl-4-nitrobenzene (>98% yield) without the use of pressured hydrogen, and the turnover frequencies (TOF) can reach 330 h^{-1}. Theoretical and experimental results reveal that the high chemo-selectivity is attributed to the preferential adsorption and activation of the Ar-C=C on the MOF-74 shell. Given its outstanding catalytic performance under mild conditions and facile preparation protocol, it would be of considerable interest to develop other MOFs@MNPs@MOFs core-shell nanocatalysts.

Keywords: Metal organic frameworks, Core-shell structure, Pd nanoparticles, Ligand exchange, Selective hydrogenation.

Introduction

Chemo-selective hydrogenation of unsaturated compounds is in widespread demand for dyes, pharmaceuticals and fine chemicals [1-5]. Efficient and highly selective reduction of C=C double bonds in the existence of other easily reducible group is necessary, especially for multi-step organic synthesis [1, 6]. Given that both C=C bonds and nitro groups, especially aromatic nitro groups, can be easily subjected to activation by common hydrogenation metal catalysts [7, 8], therein lies a long-standing challenge to promote a preferential reduction of a vinyl group (Ar-C=C) over an aryl nitro group ($Ar\text{-}NO_2$) in nitrostyrene due to the uncontrolled non-selective nature of hydrogenation under well-established conditions [6, 9, 10].

Pd NPs immobilized on microporous polymers, carbon, silica or zeolites have been regarded as efficient heterogeneous catalysts for various types of reduction reactions [11-15]. For material-supported noble-metal catalysts, the catalytic activity and selectivity are in extreme dependence on structures of the support because specific interactions take place at the interface between the active (metal) phase and the support [16, 17]. MOFs are an ideal support owing to their outstanding structures, high porosity and large specific surface area [18-20]. Encapsulation of metal NPs within MOFs has gained much attention because it not only can decrease the aggregation of metal NPs but also can provide multiple functional groups to work cooperatively with the encapsulated metal NPs, hence giving rise to higher catalytic performance [20-22]. Although loading Pd NPs on MOF is potentially useful to improve the catalytic properties, there are still several problems, such as Pd leaching and oxidation, poor dispersion, and low catalytic selectivity [23, 24]. So, there is a clear need to further optimize the synthetic strategy to address these problems.

More recently, the encapsulation of metal nanoparticles (MNPs) into a core-shell structure appears be effective in improving the stability and recyclability of catalyst [25-28]. In particularly, MOFs@MNPs@MOFs by sandwiching MNPs between two MOFs demonstrates great potential in enhancing catalytic reactivity and selectivity for

selective hydrogenation reaction [29-34]. The MOF core could act as a support, inhibiting the aggregation of metal nanoparticles. The flexible nanopores of MOFs shell can transport reactants to the active metal surface and enhance the catalyst durability. In addition, with functional groups on linkers and coordinative unsaturated metal sites (CUSs), MOF shell can serve as synergistic catalyst with metal NPs. However, only a few works have been reported yet on the use of MOFs@MNPs@MOFs for chemo-selective hydrogenation reaction. Tang and co-workers fabricated MIL-101@Pt@MIL-101 nanostructures and MIL-101@Pt@FeP-CMP catalysts for the chemo-selectivity hydrogenation of α, β-unsaturated aldehydes with significantly improved selectivity towards α, β-unsaturated alcohols [29]. Li and co-workers developed a Pt/MOFs@MOFs catalyst, which also used for the chemo-selectivity hydrogenation of C=O group over C=C bond in α, β-unsaturated aldehydes [30]. In 2020, Tang and co-workers reported that the UiO-67@Pd@UiO-67 (50 nm) was an efficient catalyst for the selective semihydrogenation of multiple alkynes [32].

Even though it was proved that sandwich structure can effectively improve the selectivity and recyclability for heterogeneous reactions, to the best of our knowledge, MOFs@MNPs@MOFs has not been used for chemo-selectivity hydrogenation of nitrostyrene. In addition, most of the MOFs@MNPs@MOFs catalysts reported in the literatures are prepared by epitaxial growth methods, and more facile fabrication methods are expected to be developed. Moreover, the unknown interactions between the MOFs framework and the MNPs also remain to be determined. The exploration of unique structure-selectivity relationship of MOFs@MNPs@MOFs nanocatalysts will provide design information for preparing more highly selective catalysts. Importantly, most hydrogenation reactions with hydrogen as reducing agent always suffer from problems of using organic solvents [8, 30], high temperature [2, 6] and high pressure [1, 6, 29, 31, 32]. From an environmental and sustainable viewpoint, water as a cheap, non-flammable and safe solvent can potentially provide an environmentally friendly and economical strategy for synthetic chemistry [1]. Therefore, it is highly desired to develop an efficient MOFs@MNPs@MOFs nanocatalyst for the chemo-selective hydrogenation of C=C bond in nitrostyrene under mild condition with water as a green solvent.

Herein, in this work, a new sandwich-structured ZIF-8@Pd@MOF-74 core-shell nanocatalyst has been designed and prepared by a simple ligand exchange method. The MOF-74 shell grown on the outer surface of the Pd/ZIF-8 core has four main functions: First, as a safe barrier to protect the Pd NPs from leaching and oxidation. Second, it can improve the dispersion of Pd NPs and allow maximum proportion of Pd NPs close to the MOFs surface. Third, it has a larger pore size than ZIF-8, which facilitates the entry and diffusion of substrate molecules to effectively contact with Pd NPs. Fourth, a proper combination of two kind of porous filter, ZIF-8 core and MOF-74 shell, gives a special microenvironment for Pd NPs, and thus, higher catalytic selectivity is expected. Our findings showed that the ZIF-8@Pd@MOF-74 nanocatalyst, when employed in the liquid-phase hydrogenation reactions, exhibited not only improved durability and recyclability, but also sought-after chemo-selectivity with water as green solvent under very mild conditions.

Experimental

Synthetic procedures

ZIF-8

ZIF-8 was synthesized according to the reported approach [35] with modifications. Briefly, 2.97 g (10 mmol) $Zn(NO_2)_3 \cdot 6H_2O$ and 1.64 g 2-methylimidazole (20 mmol) were respectively dissolved in 200 mL methanol solution. After that, the 2-methylimidazole solution was dropped into the Zn(II) solution for 0.5 h with the magnetic stirring at room temperature, aging for 24 hrs to obtain a white solid. Resulting crystal was obtained by centrifugation, washed several times with methanol, and finally vacuum-dried overnight.

ZIF-8@Pd

0.5 g of ZIF-8 was dispersed in 100 mL of DCM to obtain a uniform dispersion solution. Then 50 mg of palladium(II) acetate which dissolved in 5 mL of DCM was added into the above solution at room temperature, and stirring overnight to obtain an ivory-white solid labelled as ZIF-8@Pd^+. After centrifugation, washing, and dried

overnight, the ZIF-8@Pd^{+} was dispersed in 100 mL of Milli-Q water. Subsequently, 10 mL of $NaBH_4$ aqueous solution was slowly added into mixture along with the magnetic stirring to obtain a brown solid. After stirring for 30 min at room temperature, the solid was collected through centrifugation, washed with Milli-Q water and methanol several times respectively, and dried at 60 °C overnight to collect the final product (ZIF-8@Pd).

ZIF-8@Pd@MOF-74

The core-shell MOFs were synthesized according to the following process. 0.3 g ZIF-8@Pd was dispersed into 150 mL of methanol, then a methanol solution dissolved of 0.1 g 2,5-dihydroxyterephthalic acid (H_4dhtp) [m(ZIF-8@Pd): m(H_4dhtp)=3:1] was added. The mixture solution was stirred for 20 mins at room temperature to coating the ZIF-8@Pd core with a layer of MOF-74 shell. After that, the product was obtained after centrifugation, washed three times with methanol (50 mL), and then dried overnight. The final product was ZIF-8@Pd@MOF-74.

Catalytic activity

Performance assessment for hydrogenation reaction over ZIF-8@Pd@MOF-74: In general, catalysts containing the same amount of Pd NPs (0.3 mol%) were placed in a two-necked round-bottomed flask (25 mL), and then a balloon filled with H_2 was connected to the reaction flask. The flask was purged with H_2 for three times to allow pure H_2 atmosphere for the reaction. Subsequently, substrate (0.5 mmol) and solvents (2 mL) were injected into the flask. The catalytic hydrogenation was carried out under room temperature with a mechanical stirring. After reactions, the mixture was extracted with ethyl acetate and then the solid catalyst was obtained after centrifugation for recycle tests. The filtrate mixture was analyzed by GC–MS.

Computational methods

Density functional theory (DFT) calculations were conducted by Vienna Ab initio Simulation Package [36, 37] using GGA-PBE functional [38, 39]. The van der Waals interaction was considered by DFT-D3 method [40, 41]. The energy and force convergence criteria were set to be 1×10^{-5} eV and 0.03 eV/Å, respectively. The models for ZIF-8

and MOF were built separately due to the structure complexity. Since periodic structure of ZIF-8 includes more than 250 atoms, some N atoms which coordinated around Zn metals were saturated by methyl group to destroy its periodicity. Then the ZIF-8 model was built containing 180 atoms in one 30 Å × 30 Å × 30 Å unit cell. For reactant adsorptions, reactants were placed vertically to the plane of ZIF-8 central pore. MOF structure was modelled by a periodic structure with 162 atoms in a 26.18 Å × 26.17 Å × 6.90 Å triclinic unit cell. In MOF, reactants were parallel to the MOF plane close to Zn_3 cluster within the central pore. A (4 × 4) supercell Pd (111) slab with four layers was employed with a 5 × 5 × 1 k-point mesh for geometry optimizations. Three adsorption configurations of the reactant on Pd (111) were tested and the most stable structure was selected. The adsorption energies of adsorbates (ΔE_{ads}) was calculated as,

$$\Delta E_{ads} = E_{total} - E_{slab} - E_{adsorbate}$$

where E_{total}, E_{slab}, and $E_{adsorbate}$ represent the energies of slab with an adsorbed molecule, slab without any adsorbates, and an adsorbate, respectively.

Results and discussion

Characteristics and structure of ZIF-8@Pd@MOF-74

The schematic representation of the formation of core-shell ZIF-8@Pd@MOF-74 nanocrystal using H_4dhtp as a competitive coordination reagent was illustrated in Scheme 1. A zeolitic imidazolate framework, ZIF-8, was prepared following the procedures described previously with slight modifications [33]. Then, white ZIF-8 was dispersed in DCM solution containing $Pd(CH_3COO)_2$, and the resulting mixture was kept at room temperature for 12 hrs with mechanical perturbation. Pd(II) occupied the pores of ZIF-8 to formed the Pd(II)-loaded MOF and labeled as ZIF-8@Pd(II). After reduction by $NaBH_4$, ZIF-8@Pd (0) was obtained [17, 42], and ZIF-8@Pd@MOF-74 core-shell nanocatalyst was finally synthesized via ligand exchange method. The pore size of ZIF-8 is about 3.4 Å [43], and the smaller pore diameter can enhance the dispersion of Pd NPs effectively and decrease the particle size. The Zn-MOF-74 shell has a pore diameter approximately 10.3 Å [44], which facilitate the diffusion of the substrate and

prevent the leaching and oxidization of Pd NPs.

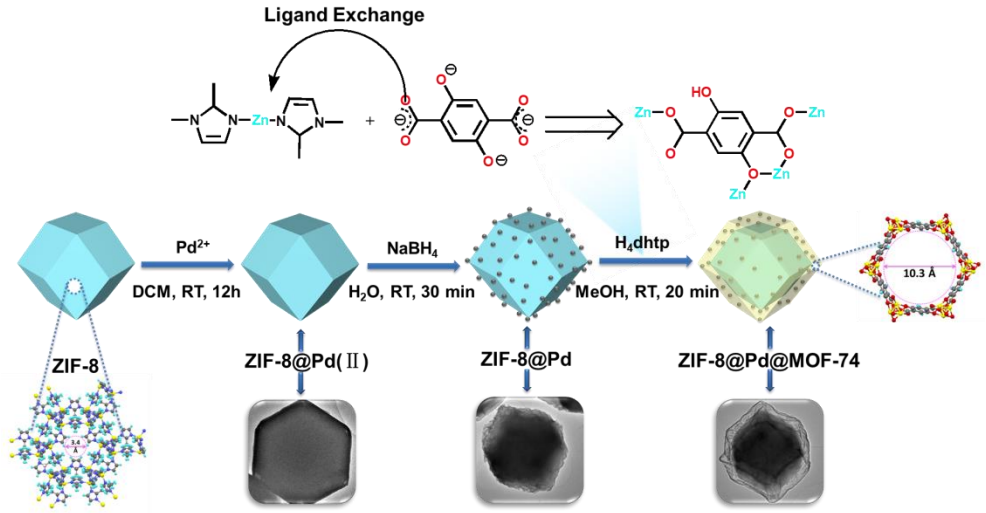

Scheme 1. Schematic synthetic process for ZIF-8@Pd@MOF-74 nanocatalyst.

The core-shell morphology was unequivocally confirmed by TEM (Fig. 1 and Fig. S1) and SEM (Fig. S2). As shown in Fig. 1a-d and Fig. S1-2, the obtained MOF was composed of dispersed crystals and uniformly sized of rhombic dodecahedral shape. The outer shell of the crystal displayed a fine raise in brightness compared with the dark inner core, which proved the core-shell structure of ZIF-8@Pd@MOF-74 (Fig. 1a). HRTEM images (Fig. S3) and Pd NPs size distribution histogram (Fig. S4) indicated that the well-dispersed Pd NPs was loaded into the ZIF-8@Pd and ZIF-8@Pd@MOF-74 with sizes range from 2.29 to 2.35 nm. Fig. 1c showed that most of the Pd NPs mainly dispersed on the surface of ZIF-8@Pd with a thickness about 20 nm. While, formation a nano-shell with a thickness of approximately 70-100 nm made Pd particles uniformly cover all over the surface of the MOF-74 shell (Fig. 1d), which may enhance active sites dispersion on the surface of core-shell catalyst. The Pd NPs was confirmed by the HRTEM image (Fig. 1e, Fig. S5), where the measured lattice spacing was 0.23 nm, corresponding to (111) facet of the face-centered cubic (FCC) Pd [45, 46], and is consistent with the reported value of Pd(0) [47]. The EDS mapping images (Fig. 1f and Fig. S6) indicated that the ZIF-8@Pd and ZIF-8@Pd@MOF-74 both contain well dispersed Pd NPs in the pore of as-prepared MOF structures. Moreover, the Pd NPs were preferentially dispersed on the shell surface of the MOF shown in Fig. 1g-h,

indicating that more Pd active sites were exposed on the surface of the core-shell ZIF-8@Pd@MOF-74 than that of ZIF-8@Pd.

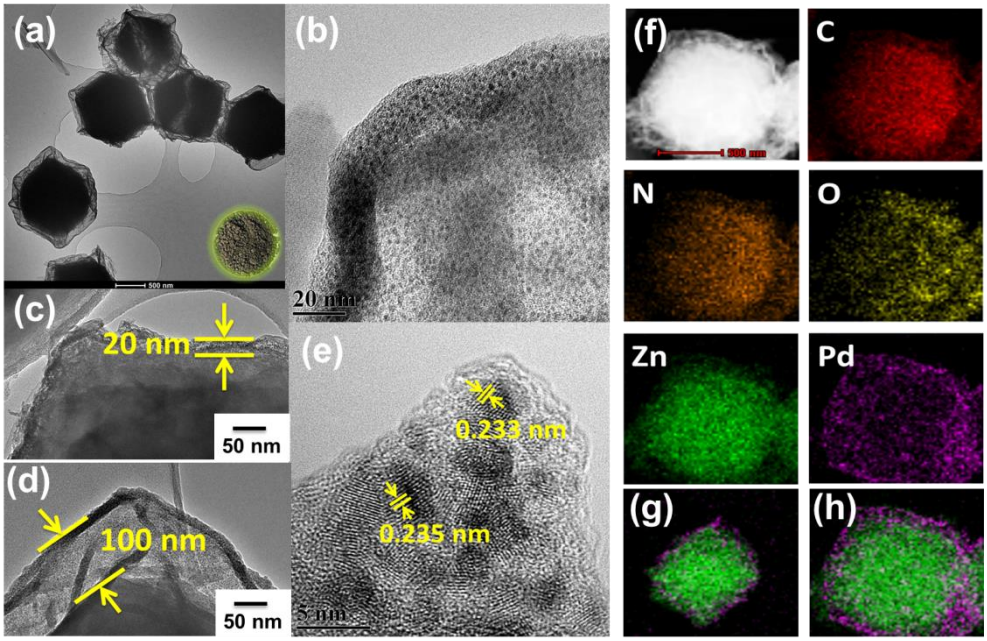

Fig. 1. (a-b) TEM images of ZIF-8@Pd@MOF-74; (c-d) Distribution of Pd NPs on the surface of ZIF-8@Pd (c) and ZIF-8@Pd@MOF-74 (d); (e) HRTEM images of ZIF-8@Pd@MOF-74; (f) TEM image and EDS elemental mapping images of a ZIF-8@Pd@MOF-74; (g-h) Overlay mapping images of ZIF-8@Pd (g) and ZIF-8@Pd@MOF-74 (h).

The agreement of the XRD patterns between the as-prepared crystal and the simulated ZIF-8 and MOF-74 further demonstrated the formation of ZIF-8@Pd@MOF-74 structure and the well-maintained frameworks of ZIF-8 during the Pd loading and reducing processes (Fig. 2a). For ZIF-8@Pd@MOF-74, the peaks around 6.9° and 11.8° can be assigned to (110) and (300) crystal planes of MOF-74 [18,19], indicating the formation of the MOF-74 shell. In addition, ZIF-8@Pd@MOF-74 has characteristic IR absorbance peaks of ZIF-8, and there are several additional peaks in range of 700-1800 cm^{-1} contributed to the MOF-74 (Fig. 2b) [48], which further proved the formation of MOF-74 shell. No characteristic peaks for Pd NPs were observed most probably due to the low loading in the MOFs. The existence of Pd(0) and the chemical state of as-prepared material were also confirmed by the XPS analyses.

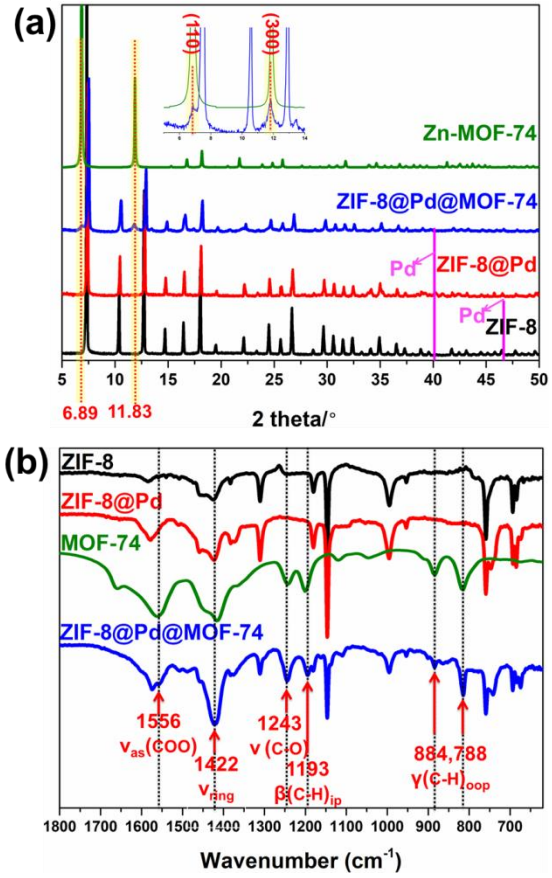

Fig. 2. (a) PXRD patterns and (b) FTIR spectra of ZIF-8, Zn-MOF-74, ZIF-8@Pd and ZIF-8@Pd@MOF-74.

Fig. 3a showed the XPS survey spectrum of the three kinds of MOF structures, and the emergence of the new peak at 300-400 eV confirmed the successful loading of Pd NPs in the ZIF-8@Pd and ZIF-8@Pd@MOF-74. The Pd 3d region of ZIF-8@Pd@MOF-74 (Fig. 3b) displayed two main peaks at 335.7 and 340.9 eV as well as two small peaks at 338.1 and 343.2 eV, which could be attributed to Pd $3d_{5/2}$ and Pd $3d_{3/2}$ of Pd(0) and Pd(II), respectively [49-51]. The appearance of the Pd(II) peak might be caused by the surface oxidation of Pd(0) NPs [49, 50]. The Pd 3d spectrum of ZIF-8@Pd showed that the surface of Pd NPs mainly existed in the divalent state, indicating that the Pd(0) on the core-shell ZIF-8@Pd@MOF-74 surface was less easily oxidized than that of ZIF-8@Pd due to the presence of the MOF-74 shell. Meanwhile, N 1s and O 1s images showed in Fig. S7 demonstrated the oxygen increase significantly with the decrease in nitrogen for the ZIF-8@Pd@MOF-74 nanocrystal, confirming the ligand

exchange of 2-MI and H4dhtp.

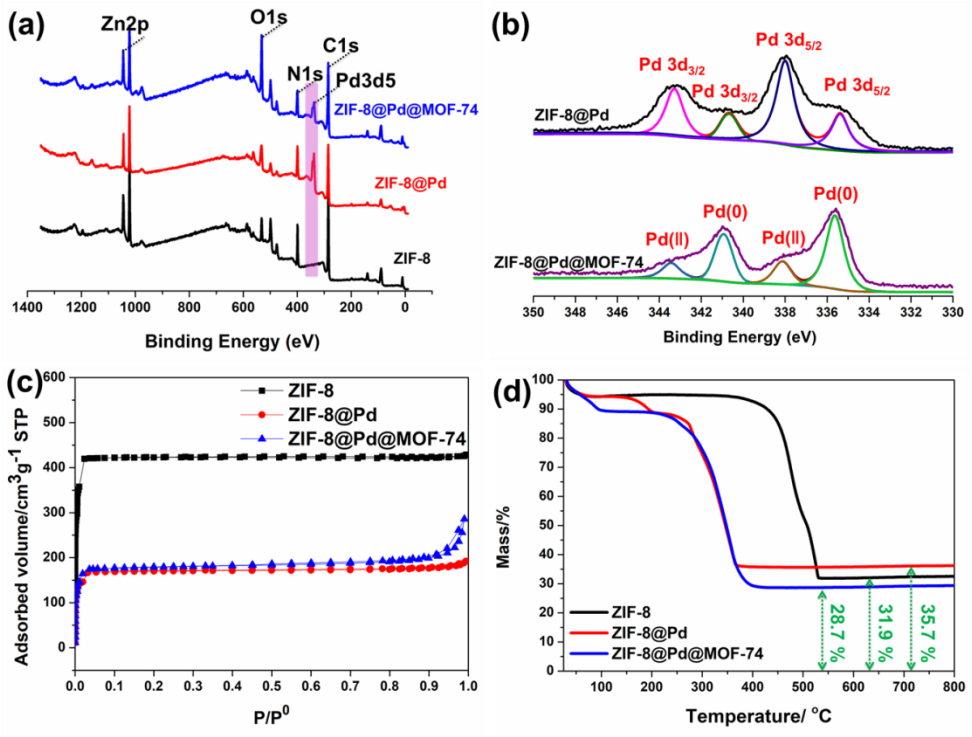

Fig. 3. (a) The XPS survey spectrum of the ZIF-8, ZIF-8@Pd and ZIF-8@Pd@MOF-74; (b) the XPS Pd 3d spectrum of ZIF-8@Pd and ZIF-8@Pd@MOF-74; (c) N_2 adsorption/desorption isotherms and (d) TGA images of the ZIF-8, ZIF-8@Pd and ZIF-8@Pd@MOF-74.

The Brunauer-Emmett-Teller (BET) specific surface area and porosity of the MOFs were characterized with N_2 adsorption-desorption isotherms (Fig. 3c and Fig. S8). ZIF-8, ZIF-8@Pd and ZIF-8@Pd@MOF-74 all showed fully reversible type I N_2 sorption isotherms at a relative pressure from 0.1 to 1.0 (Fig. 3c) [52, 53]. The BET surface area of ZIF-8@Pd@MOF-74 was calculated to be 727 $m^2 \cdot g^{-1}$, which was lower than that of ZIF-8 (1744 $m^2 \cdot g^{-1}$) (Table S1), and a decrease in specific surface area associated with the loading of Pd NPs, indicating that the Pd NPs were loaded inside the pores of MOFs. Table S1 showed that Zn-MOF-74@Pd has a larger pore size, implying that the surface coating MOF-74 contributes to improve the specific surface area and pore size of ZIF-8@Pd@MOF-74 compared to ZIF-8@Pd. The elemental composition of the materials was confirmed by ICP-OES (Table S2) and EDS (Fig. 3c and Fig. S9). It can be observed that the Pd loading was 4.6 wt% and 4.2 wt% respectively for ZIF-8@Pd and

ZIF-8@Pd@MOF-74 from table S2. The contents of Zn and Pd in the core-shell MOF decreased due to the addition of H_4dhtp ligand, which also be proved by EDS (Fig. S9) and TGA (Fig. 3d) results. However, the Pd loading in Zn-MOF-74 was only 0.7 wt % due to the lower BET capacity, confirming the advantages of preparation the core-shell MOFs with different pore diameters.

Chemo-selective hydrogenation reactions

The catalytic performance of as-prepared ZIF-8@Pd@MOF-74 nanocatalyst was investigated for chemo-selective hydrogenation of Ar-C=C to Ar-C-C in the presence of Ar-NO_2. 4-nitrostyrene (NS, 1a) was chosen as a model molecule to investigate the chemo-selectivity of different catalysts. The ZIF-8, Zn-MOF-74 and ZIF-8@Pd(II) were almost inactive (entry 2-4), which confirmed that Pd(0) is necessary for the hydrogenation of nitrostyrene. It indicates from table 1 that all Pd-loaded catalysts showed high conversion and selectivity to the reduction of unsaturated C=C bonds in hydrogenation of 4-nitrostyrene. Particularly, ZIF-8@Pd@MOF-74 exhibited an outstanding chemo-selectivity (>98% yield, entry 7) to 1-ethyl-4-nitrobenzene (1b) at almost 100% conversion of NS at 298 K within 1 h with a H_2 balloon. Although the conversion of Pd/C was almost the same as that of ZIF-8@Pd@MOF-74, the selectivity of Pd/C was not good (84%) (entry 1). The selectivity of ZIF-8@Pd@MOF-74 catalyst was also superior to ZIF-8@Pd (entry 6) and Zn-MOF-74@Pd (entry 5, structure confirmed by XRD Fig. S10), and no 4-vinylaniline (1c) was detected. In addition, it was found that the reaction time had a greater influence on the selectivity of Pd/C and ZIF-8@Pd (Fig. S11). A mixture of two reduction products (4-ethylaniline, and 1-ethyl-4-nitrobenzene) was afforded in a higher conversion with a prolonged reaction time.

The chemo-selective hydrogenation with ZIF-8@Pd@MOF-74 nanocatalysts under different solvents were compared (Table 1, entries 8-12). The core-shell catalyst displayed higher selectivity to the hydrogenation of unsaturated C=C bonds than the aromatic nitro group under all six solvents. When the solvent polarity increases, the conversion becomes higher. The protic solvents are more conducive to the improvement of reaction efficiency because of water is easily forms hydrogen bonds with the nitro

group in nitrostyrene at the interface [54]. The nitro group protruded outwards to improve their water solubility, while the C=C bond closer to the active Pd catalytic center of ZIF-8@Pd@MOF-74 to facilitate its preferential hydrogenation. Compared with the Pd-supported catalyst for chemo-selectivity hydrogenation of nitrostyrene reported in the literature (Table S3), the ZIF-8@Pd@MOF-74 catalyst exhibited higher conversion (TOF is 330 h^{-1}) and excellent selectivity to Ar-C=C bond under milder conditions, such as room temperature, one atmosphere and water as the solvent.

The hydrogenation of 3-nitrostyrene and other nitroarenes that contain Ar-NO_2 and Ar-C=O under the same conditions was tested to further evaluate whether coating MOF-74 on ZIF-8@Pd can improve its catalytic performance. As can be seen from Table 1, ZIF-8@Pd@MOF-74 showed good selectivity compared with ZIF-8@Pd and Pd/C, catalyzing the hydrogenation of 3-nitrostyrene directly to 1-Ethyl-3-nitrobenzene (>98% yield within 1.5 h) (entries 13-15). When Ar-NO_2 coexists with Ar-C=O, ZIF-8@Pd@MOF-74 catalyst exhibited outstanding chemo-selective hydrogenation of Ar-NO_2 to Ar-NH_2 than ZIF-8@Pd for 4-Nitrobenzaldehyde (entries 16-17), 4-Nitroacetophenone (entries 18-19) and 2-Bromo-4'-nitroacetophenone can also afford the desired aromatic amine (entries 20-21). The selective hydrogenation of the nitro group in the coexistence with the carbonyl may be the preferential adsorption and activation of nitro groups by MOF. It was noteworthy that the conversion on ZIF-8 was lower than that of core-shell MOFs. A possible reason was the imidazole fragment may shield some channels to hinder substrate molecules passing through [55]. Another reason was that the Pd on the surface of ZIF-8@Pd easily oxidized, which would limit the catalytic efficacy mainly occurring on its external surface.

Table 1. The catalytic performance of Pd-supported catalysts for chemoselective hydrogenation of nitroarenes.

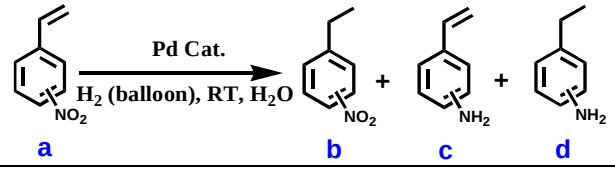

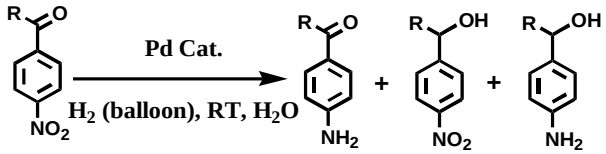

Entry	Catalysts	Time (h)	Solvents	Conversion (%)	Yield (%)		
					b/B	c/C	d/D
Substrate: 4-Nitrostyrene							
1	Pd/C	1	H_2O	99	83	-	16
2	ZIF-8	1	H_2O	Trace	-	-	-
3	Zn-MOF-74	1	H_2O	Trace	-	-	-
4	ZIF-8@Pd(II)	1	H_2O	Trace	-	-	-
5	Zn-MOF-74@Pd	1	H_2O	86	86	-	-
6	ZIF-8@Pd	1	H_2O	91	84	-	7
7	ZIF-8@Pd@ MOF-74	1	H_2O	99	98	-	1
8	ZIF-8@Pd@ MOF-74	1	MeOH	100	99	-	1
9	ZIF-8@Pd@ MOF-74	1	EtOH	100	99	-	1
10	ZIF-8@Pd@ MOF-74	1	EA	99	98	-	1
11	ZIF-8@Pd@ MOF-74	1	DCM	95	94	-	1
12	ZIF-8@Pd@ MOF-74	1	PE	89	88	-	1
Substrate: 3-Nitrostyrene							
13	Pd/C	1.5	H_2O	99	88	-	11
14	ZIF-8@Pd	1.5	H_2O	93	87	-	6
15	ZIF-8@Pd@ MOF-74	1.5	H_2O	99	98	-	1
Substrate: 4-Nitrobenzaldehyde							
16	ZIF-8@Pd	5	H_2O	95	95	-	-
17	ZIF-8@Pd@ MOF-74	5	H_2O	99	99	-	-
Substrate: 4-Nitroacetophenone							
18	ZIF-8@Pd	2	H_2O	94	94	-	-
19	ZIF-8@Pd@ MOF-74	2	H_2O	99	99	-	-
Substrate: 2-Bromo-4'-nitroacetophenone							
20	ZIF-8@Pd	1.5	H_2O	95	95	-	-
21	ZIF-8@Pd@ MOF-74	1.5	H_2O	99	99	-	-

Reaction conditions: Substrates (0.5 mmol), Pd cat. (Pd 0.3 mol %), Solvent (2 mL), H_2 (Hydrogen balloon), Room temperature. Yields were determined by GC-MS.

DFT calculation and mechanism analysis

To explain the higher selectivity of the core-shell ZIF-8@Pd@MOF-74, one can assume that the intrinsic rate for the hydrogenation of the C=C double bond on the catalyst is responsible for the high chemoselectivity observed. To check this hypothesis, DFT calculations were conducted to study MOF and ZIF contributions to the catalytic

activity and selectivity. Since the catalytic reactions mainly occurred on the outer surface of catalysts, reaction energies were calculated on the shells (Zn-MOF-74 in ZIF-8@Pd@MOF-74, and ZIF-8 in ZIF-8@Pd). The calculated reaction energy for the hydrogenation reaction from 1a to 1b on Zn-MOF-74 was -1.57 eV, which was much lower than that in the reaction from 1a to 1c (0.31 eV), indicating that 1b was energetically favored compared to 1c (Fig. S12). In the case of ZIF-8 as shown in Fig. S13, the calculated reaction energies for 1b and 1c as reaction products were -1.60 eV and 0.14 eV, respectively, which showed a smaller difference in the selectivity of 1b over 1c. These results indicated that the hydrogenation of C=C bond was thermodynamically favored compared to the nitro group.

A second assumption is that there might be a synergistic effect between Pd and MOFs, where H_2 dissociates on Pd and nitrostyrene (NS) is preferentially adsorbed on the MOF support through the C=C double bonds [29]. Therefore, to illustrate the high selectivity of ZIF-8@Pd@MOF-74, the adsorption orientations for NS on Zn-MOF-74 and ZIF-8 were considered [16, 56] and shown in Fig. 4. According to calculation results, the adsorption energy of NS (-0.85 eV) on Zn-MOF-74 with the vinyl-oriented Zn cluster (denoted as VOZM, Fig. 4a) was stronger than that on ZIF-8 (-0.55 eV, denoted as VOZF shown in Fig. 4b and Fig. S14), which demonstrated that Zn-MOF-74 has higher selectivity to activate the vinyl group. One possible reason is that four-coordinated Zn atoms are fully connected with N atoms in ZIF-8 [55], preventing NS from approaching to zinc atom. But the infinite helical rods of $Zn_3[O_3(CO_2)_3]$ including coordinatively unsaturated metal sites (CUSs) in Zn-MOF-74 could create open sites without repulsive force of ligands [55], which can facilitate the reaction with NS by the electron transfer. Previous study demonstrated that, CUSs inside MOFs could act as Lewis acid sites, activating targeted chemical bonds and lowering the reaction energy barrier of the desired chemical transformation, which also support our results [29]. Therefore, CUSs in Zn-MOF-74 play an important role in selectively facilitating hydrogenating of C=C bond.

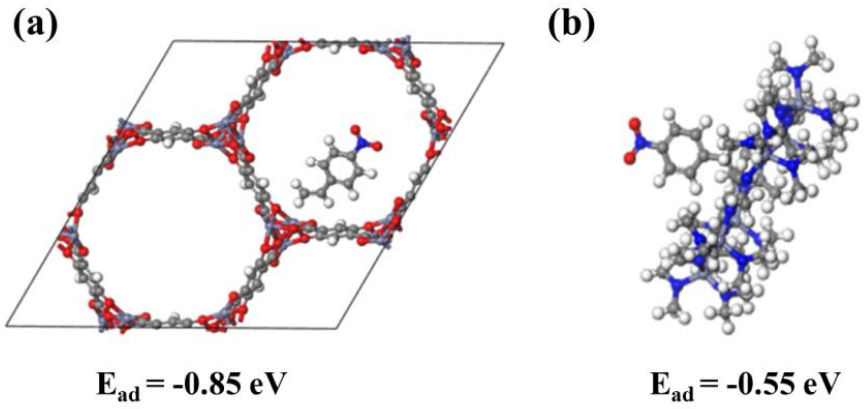

Fig. 4. (a) The binding energies for vinyl-oriented Zn cluster in MOF-74 (VOZM); (b) The binding energies for vinyl-oriented Zn cluster in ZIF-8 (VOZF).

This conclusion was further supported by XPS results. As shown in Fig. 5, there was a positive shift in the binding energy of Zn 2p spectra from 1021.5 to 1021.8 eV and 1044.6 to 1044.9 eV after the formation of core-shell MOF by ligand exchange (Fig. 5a). This shift indicated a decrease in electron density around Zn atoms due to the high negative charge residing on the compact dtp^{4-} ligand [57, 58]. CUSs atom with a positive charge prefers to approach C=C bond with π electrons, and in turn improved the adsorption of vinyl group in NS [57]. Also, the binding energy of Pd 3d was shift to higher value (Fig. 5b), which indicated that the surrounding environment has a strong influence on the electronic states of the enclosed palladium clusters, and the decrease in electron density around Zn atoms makes a partial transfer of electrons from the Pd nanoparticles to ZIF-8@Pd@MOF-74 [29]. The reduced electron density of Pd nanoparticles may affect the hydrogenation activity. As a consequence, the catalytic selectivity is determined by constituents of core and shell, and the CUSs atom with a positive charge in the MOF-74 can preferentially adsorb the C=C double bond and activate it.

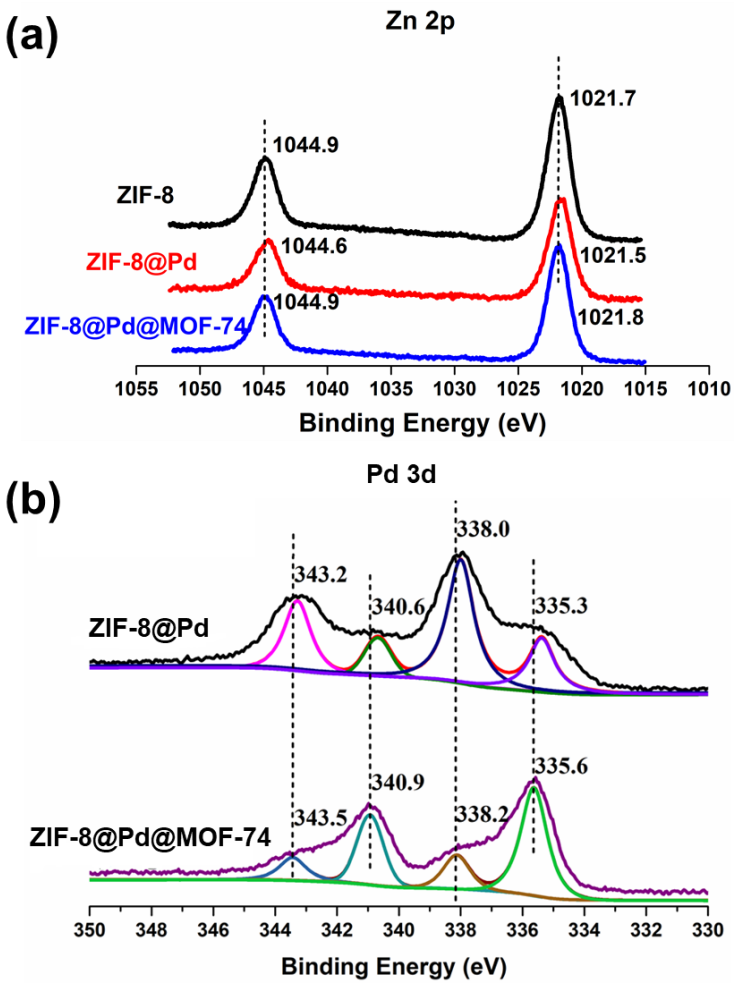

Fig. 5. (a) XPS Zn 2p spectrum of ZIF-8, ZIF-8@Pd and ZIF-8@Pd@MOF-74; (b) XPS Pd 3d spectrum of ZIF-8@Pd and ZIF-8@Pd@MOF-74.

The catalytic selectivity of Pd nanoparticles was also investigated by DFT calculations. Three adsorption configurations for NS on Pd (111) surface are shown in Fig. 6. The adsorption energies for vinyl group contacting with Pd (Fig. 6a), nitryl group contacting with Pd (Fig. 6b), and parallel adsorption (Fig. 6c) were -0.001 eV, -0.323 eV, and -1.346 eV, respectively. Thus, the parallel adsorption structure with the largest binding energy was selected for further investigation. Based on our results (Fig. 7), the reaction energy from 1a to 1b on Pd (111) was -0.85 eV (Fig. 7a), while the reaction energy from 1a to 1c on Pd (111) was -0.046 eV (Fig. 7b), illustrating that reaction from 1a to 1b is more favorable on Pd (111). This conclusion is also consistent with the experimental observation that the CUSs in Zn-MOF-74 preferentially interacted with the C=C group (rather than the NO_2 group) of NS. Based on the DFT calculations, one

can conclude that the high chemo-selectivity obtained with ZIF-8@Pd@MOF-74 not only is due to a higher intrinsic activity for hydrogenating the C=C bond with respect to the nitro group, but also is a consequence of the preferential adsorption and activation of the C=C bond on the MOF-74 shell.

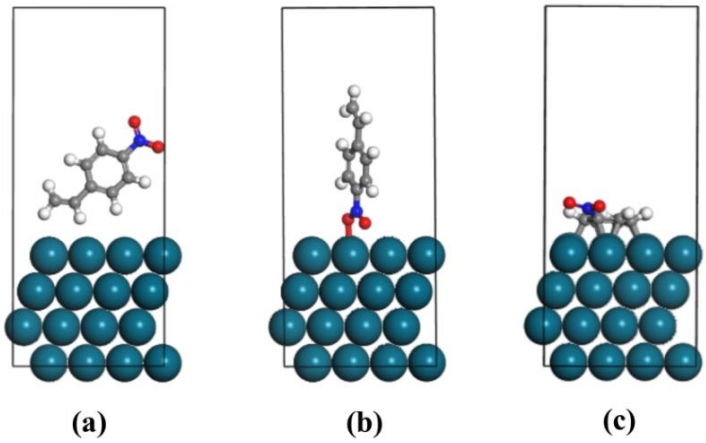

Fig. 6. Three adsorption configurations for nitrostyrene (NS) on Pd (111) surface: (a) vinyl group contacting with Pd (111); (b) nitryl group contacting with Pd (111); (c) parallel adsorption.

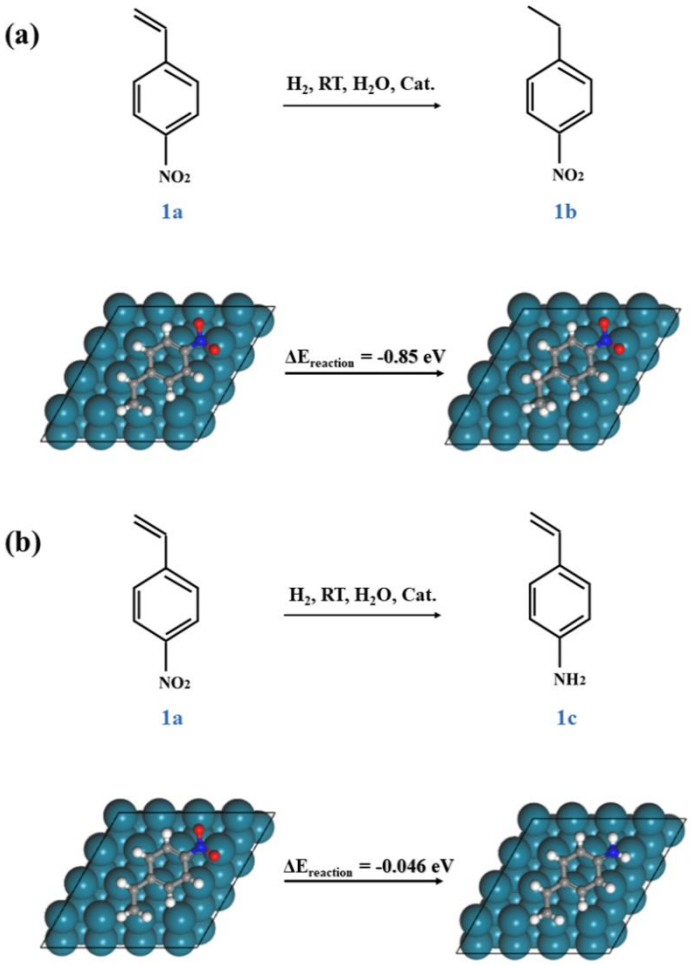

Fig. 7. (a) Reaction process from 1a to 1b on Pd (111); (b) reaction process from 1a to 1c on Pd (111).

Cyclic stability

The stability of ZIF-8@Pd@MOF-74 nanocatalyst was tested for the chemo-selective hydrogenation of NS. The catalyst was recovered by simple centrifugation followed by washing with water/methanol. As can be seen from Fig. 8a, ZIF-8@Pd@MOF-74 showed an excellent reusability, and the yield of 1b still can up to 84% after five catalytic cycles. In stark contrast, the catalytic activity of ZIF-8@Pd obviously decreased as the number of cycles increased. The Pd leaching results in Table S4 proved that the MOF-74 shell can prevent Pd nanoparticles from leaching. However, the collapse of crystal surface may be caused by mechanical agitation or some reactants and products react with MOFs (Fig. S15). PXRD patterns confirmed the structural integrity after reaction (Fig. S16). The XPS Zn 2p and Pd 3d patterns of the reused ZIF-

8@Pd@MOF-74 showed a negative shift compared to the fresh catalyst (Fig. 8b-c), which may be caused by the adsorption both the aromatic ring and the C=C double bond. The change in binding energy was consistent with the DFT conclusion that the C=C double bond preferentially adsorbs on the CUSs, and NS was parallel adsorbed on the Pd (111) surface. Fig. S17 demonstrated that the MOF-74 shell can prevent the oxidation of Pd, and there was no significant increase of Pd in divalent state after reaction. The IR spectrum did not change significantly before and after the reaction, but the C-H bond peak of NS appeared at around 2900 cm^{-1} (Fig. 8d), which proved the existence of coordination between NS and the catalyst. Therefore, ZIF-8@Pd@MOF-74 demonstrates better stability and recyclability due to the MOF-74 shell prevent Pd NPs from leaching, oxidation, and poisoning owing to the chemisorbed impurity molecules caused by direct exposure to the catalytic environment.

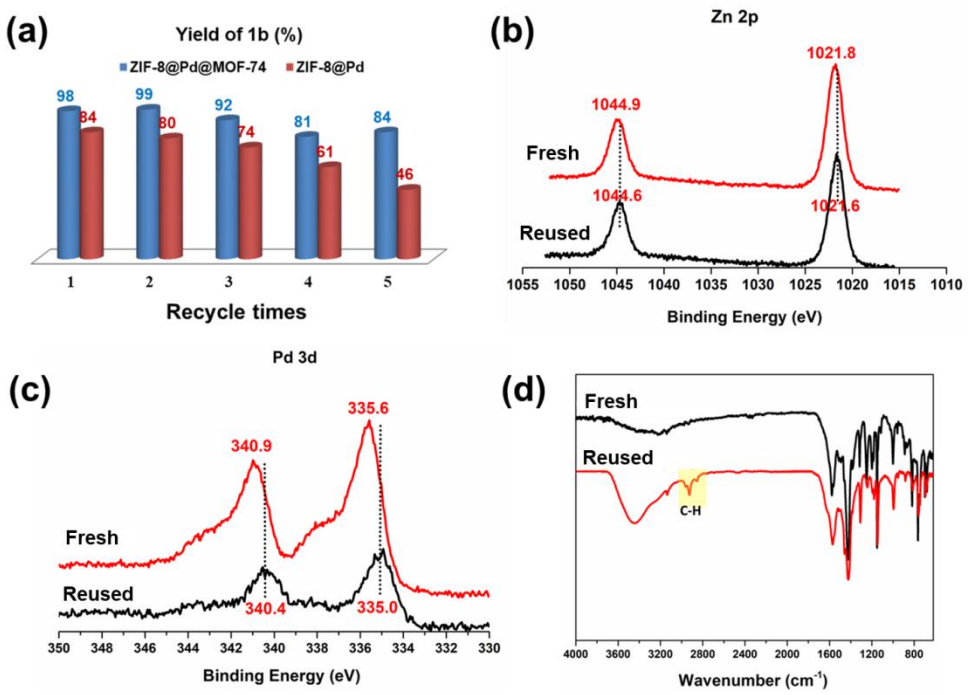

Fig. 8. (a) The recycle performance of ZIF-8@Pd@MOF-74 and ZIF-8@Pd for hydrogenation of NS; (b) The XPS Zn 2p spectrums and (c) Pd 3d spectrum of fresh and reused ZIF-8@Pd@MOF-74; (d) FT-IR results of fresh and reused ZIF-8@Pd@MOF-74.

Conclusion

A new Pd-loaded core-shell ZIF-8@Pd@MOF-74 nanocatalyst for chemo-selective hydrogenation of Ar-C=C in the present of Ar-NO_2 was synthesized by combining two kinds of MOFs with different pore sizes. The ZIF-8 core is beneficial for improving the loading and dispersibility of Pd NPs, while, the outer MOF-74 shell benefits improves the durability of Pd catalyst. The catalytic activity and selectivity (99%) for the C=C bond of NS was significantly improved on ZIF-8@Pd@MOF-74 nanocatalyst compared with other Pd-supported ones. More importantly, compared with the Pd-catalyzed nitrostyrene reaction reported in the literature, the developed catalytic system can be efficiently performed with water as a solvent at room temperature and 1 atm. The role of outer shell in nitrostyrene hydrogenation reactions was systematically investigated via experimental and computational approaches, and the proposed the preferential adsorption and activation of the Ar-C=C than Ar-NO_2 on the MOF-74 shell contribute to the higher selectivity. This facile preparation strategy can provide a solid blueprint to prepare other metal-loaded core-shell MOFs for hydrogenation reactions under milder conditions.

Acknowledgment

This work is financially supported by the Hong Kong Research Grants Council, Area of Excellence Grants (1-ZVGG) of Hong Kong Polytechnic University (No. PolyU 153012/15P); Basic Research Program of Shenzhen Grants (No. JCYJ20160531184120814); The Startup Fund from the Hong Kong University of Science and Technology.

Supporting Data

Supplementary characterizations for ZIF-8, ZIF-8@Pd and ZIF-8@Pd@MOF-74 including TEM, SEM, HRTEM, XRD, etc.

Reference

(1) Trandafir, M. M.; Pop, L.; Hădade, N. D.; Florea, M.; Neațu, F.; Teodorescu, C. M.; Duraki, B.; van Bokhoven, J. A.; Grosu, I.; Pârvulescu V. I.; Garcia, H. An Adamantane-Based COF: Stability, Adsorption Capability, and Behaviour as a

Catalyst and Support for Pd and Au for The Hydrogenation of Nitrostyrene. *Catal. Sci. Technol.* **2016**, *6*, 8344-8354.

(2) Camacho-Bunquin, J.; Ferrandon, M.; Sohn, H.; Yang, D.; Liu, C.; Leon, P. A. I.; Perras, F. A.; Pruski, M.; Stair, P. C.; Delferro, M. Chemoselective Hydrogenation with Supported Organoplatinum(IV) Catalyst on Zn(II)-Modified Silica. *J. Am. Chem. Soc.* **2018**, *140*, 3940-3951.

(3) Yang, N.; Cheng, H.; Liu, X.; Yun, Q.; Chen, Y.; Li, B.; Chen, Bo.; Zhang, Z.; Chen, X.; Lu, Q.; Huang, J.; Huang, Y.; Zong, Y.; Yang, Y.; Gu, L.; Zhang H. Amorphous/Crystalline Hetero-Phase Pd Nanosheets: One-Pot Synthesis and Highly Selective Hydrogenation Reaction. *Adv. Mater.* **2018**, *30*, 1803234.

(4) Gu, J.; Zhang, Z.; Hu, P.; Ding, L.; Xue, N.; Peng, L.; Guo, X.; Lin, M.; Ding W. Platinum Nanoparticles Encapsulated in MFI Zeolite Crystals by a Two-Step Dry Gel Conversion Method as a Highly Selective Hydrogenation Catalyst. *ACS Catal.* **2015**, *5*, 6893-6901.

(5) Shen, M.; Liu, Hu.; Yu, C.; Yin, Z.; Muzzio, M.; Li, J.; Xi, Z.; Yu, Y.; Sun S. Room-Temperature Chemoselective Reduction of 3-nitrostyrene to 3-vinylaniline by Ammonia Borane over Cu Nanoparticles. *J. Am. Chem. Soc.* **2018**, *140*, 16460-16463.

(6) Mahata, N.; Cunha, A. F.; Órfão, J. J. M.; Figueiredo, J. L. Highly Selective Hydrogenation of C-C Double Bond in Unsaturated Carbonyl Compounds over NiC Catalyst. *Chem. Eng. J.* **2012**, *188*, 155-159.

(7) Corma, A.; Serna, P.; Concepcio´n, P.; Calvino J. J. Transforming Nonselective into Chemoselective Metal Catalysts for the Hydrogenation of Substituted Nitroaromatics. *J. Am. Chem. Soc.* **2008**, *130*, 8748-8753.

(8) Beier, M. J.; Andanson, J. M.; Baiker, A. Tuning the Chemoselective Hydrogenation of Nitrostyrenes Catalyzed by Ionic Liquid-Supported Platinum Nanoparticles. *ACS Catal.* **2012**, *2*, 2587-2595.

(9) Høja, M.; Lindea, K.; Hansena, T. K.; Brorsonb, M.; Jensena, A. D.; Grunwaldt, J. D. Flame Spray Synthesis of CoMo/Al_2O_3 Hydrotreating Catalysts. *Appl. Catal. A-Gen.* **2011**, *397*, 201-208.

(10) Shen, M.; Liu, H.; Yu, C.; Yin, Z.; Muzzio, M.; Li, J.; Xi, Z.; Yu, Y.; Sun, S. Room-Temperature Chemoselective Reduction of 3-nitrostyrene to 3-vinylaniline by Ammonia Borane over Cu Nanoparticles. *J. Am. Chem. Soc.* **2018**, *140*, 16460-16463.

(11) Zhang, T.; Zhang, X.; Yan, X.; Lin, L.; Liu, H.; Qiu, J.; Yeung, K. L. Core-Shell Pd/ZSM-5@ZIF-8 Membrane Micro-Reactors with Size Selectivity Properties for Alkene Hydrogenation. *Catal. Today.* **2014**, *236*, 41-48.

(12) Veerakumar, P.; Thanasekaran, P.; Lu, K. L.; Liu, S. B.; Rajagopal, S. Functionalized Silica Matrices and Palladium: A Versatile Heterogeneous Catalyst for Suzuki, Heck, and Sonogashira Reactions. *ACS Sustainable Chem. Eng.* **2017**, 5, 6357-6376.

(13) Zhu, Q. L.; Tsumori, N.; Xu, Q. Immobilizing Extremely Catalytically Active Palladium Nanoparticles to Carbon Nanospheres: A Weakly-Capping Growth Approach. *J. Am. Chem. Soc.* **2015**, *137*, 11743-11748.

(14) Wang, Z. J.; Ghasimi, S.; Landfester, K.; Zhang, K. A. I. Photocatalytic Suzuki Coupling Reaction Using Conjugated Microporous Polymer with Immobilized Palladium Nanoparticles under Visible Light. *Chem. Mater.* **2015**, *27*, 1921-1924.
(15) Feng, Q.; Zhao, S.; Wang, Y.; Dong, J.; Chen, W.; He, D.; Wang, D.; Yang, J.; Zhu, Y.; Zhu, H.; Gu, L.; Li, Z.; Liu, Y.; Yu, R.; Li, J.; Li, Y. Isolated Single-Atom Pd Sites in Intermetallic Nanostructures: High Catalytic Selectivity for Semihydrogenation of Alkynes. *J. Am. Chem. Soc.* **2017**, *139*, 7294-7301.
(16) Boronat, M.; Concepcio´ n, P.; Corma, A.; Gonza´ lez, S.; Illas, F.; Serna, P. A Molecular Mechanism for the Chemoselective Hydrogenation of Substituted Nitroaromatics with Nanoparticles of Gold on TiO_2 Catalysts: A Cooperative Effect between Gold and the Support. *J. Am. Chem. Soc.* **2007**, *129*, 16230-16237.
(17) Tan, Y.; Liu, X. Y.; Li, L.; Kang, L.; Wang, A.; Zhang, T. Effects of Divalent Metal Ions of Hydrotalcites on Catalytic Behavior of Supported Gold Nanocatalysts for Chemoselective Hydrogenation of 3-nitrostyrene. *J. Catal.* **2018**, *364*, 174-182.
(18) Guo, C.; Zhang, Y.; Guo, Y.; Zhang, L.; Zhang, Y.; Wang, J. A General and Efficient Approach for Tuning the Crystal Morphology of Classical MOFs. *Chem. Commun.* **2018**, *54*, 252-255.
(19) Guo, C.; Zhang, Y.; Zhang, Y.; Wang, J. An Efficient Approach for Enhancing the Catalytic Activity of Ni-MOF-74 via a Relay Catalyst System for the Selective Oxidation of Benzylic C-H Bonds under Mild Conditions. *Chem. Commun.* **2018**, *54*, 3701-3704.
(20) Yang, Q.; Xu, Q.; Jiang H. L. Metal-Organic Frameworks Meet Metal Nanoparticles: Synergistic Effect for Enhanced Catalysis. *Chem. Soc. Rev.* **2017**, *46*, 4774-4808.
(21) Zhang, W.; Lu, G.; Cui, C.; Liu, Y.; Li, S.; Yan, W.; Xing, C.; Chi, Y. R.; Yang, Ya.; Huo, F. A Family of Metal-Organic Frameworks Exhibiting Size-Selective Catalysis with Encapsulated Noble-Metal Nanoparticles. *Adv. Mater.* **2014**, *26*, 4056-4060.
(22) Zhao, M.; Deng, K.; He, L.; Liu, Y.; Li, G.; Zhao, H.; Tang, Z. Core-Shell Palladium Nanoparticle@Metal-Organic Frameworks as Multifunctional Catalysts for Cascade Reactions. *J. Am. Chem. Soc.* **2014**, *136*, 1738-1741.
(23) Zhang, T.; Li, B.; Zhang, X.; Qiu, J.; Han, W.; Yeung, K. L. Pd Nanoparticles Immobilized in a Microporous/Mesoporous Composite ZIF-8/MSS: A Multifunctional Catalyst for the Hydrogenation of Alkenes. *Micropor. Mesopor. Mat.* **2014**, *197*, 324-330.
(24) Yang, Q.; Yao, F.; Zhong, Y.; Chen, F.; Shu, X.; Sun, J.; He, L.; Wu, B.; Hou, K.; Wang, D.; Li, X. Metal-Organic Framework Supported Palladium Nanoparticles: Applications and Mechanisms. Part. *Part. Syst. Charact.* **2019**, *36*, 1800557.
(25) Lin, L.; Zhang, T.; Liu, H.; Qiu, J.; Zhang X. In Situ Fabrication of a Perfect Pd/ZnO@ZIF-8 Core-Shell Microsphere as an Efficient Catalyst by a ZnO Support-Induced ZIF-8 Growth Strategy. *Nanoscale*. **2015**, *7*, 7615-7623.
(26) Li, Z.; Zeng, H. C. Surface and Bulk Integrations of Single-Layered Au or Ag Nanoparticles onto Designated Crystal Planes {110} or {100} of ZIF-8. *Chem. Mater.* **2013**, *25*, 1761-1768.

(27) Zhang, T.; Lin, L.; Zhang, X.; Liu, H.; Yan, X. Liu, Z.; Yeung, K. L. Facile Preparation of ZIF-8@Pd-CSS Sandwich-type Microspheres via in situ Growth of ZIF-8 Shells over Pd-loaded Colloidal Carbon Sphereswith Aggregation-Resistant and Leach-Proof Properties for the Pd Nanoparticles. *Appl. Surf. Sci.* **2015**, *351*, 1184-1190.

(28) Tang, J.; Salunkhe, R. R.; Liu, J.; Torad, N. L.; Imura, M.; Furukawa, S.; Yamauchi, Y. Thermal Conversion of Core-Shell Metal-Organic Frameworks: A New Method for Selectively Functionalized Nanoporous Hybrid Carbon. *J. Am. Chem. Soc.* **2015**, *137*, 1572-1580.

(29) Zhao, M.; Yuan, K.; Wang, Y.; Li, G.; Guo, J.; Gu, L.; Hu, W.; Zhao, H; Tang, Z. Metal-Organic Frameworks as Selectivity Regulators for Hydrogenation Reactions. *Nature*. **2016**, *539*, 77-80.

(30) Liu, H.; Chang, L.; Chen, L.; Li, Y. Nanocomposites of Platinum/Metal-Organic Frameworks Coated with Metal-Organic Frameworks with Remarkably Enhanced Chemoselectivity for Cinnamaldehyde Hydrogenation. *ChemCatChem*. **2016**, *8*, 946-951.

(31) Yuan, K.; Song, T.; Wang, D.; Zhang, X.; Gao, X.; Zou, Y.; Dong, H.; Tang, Z.; Hu, W. Effective and Selective Catalysts for Cinnamaldehyde Hydrogenation: Hydrophobic Hybrids of Metal-Organic Frameworks, Metal Nanoparticles, and Micro- and Mesoporous Polymers. *Angew. Chem. Int. Ed.* **2018**, *57*, 5708-5713.

(32) Choe, K.; Zheng, F.; Wang, H.; Yuan, Y.; Zhao, W.; Xue, G.; Qiu, X.; Ri, M.; Shi, X.; Wang, Y.; Li, G.; Tang, Z. Fast and Selective Semihydrogenation of Alkynes by Palladium Nanoparticles Sandwiched in Metal-Organic Frameworks. *Angew. Chem. Int. Ed.* **2020**, *59*, 3650-3657.

(33) Wan, M.; Zhang, X.; Li, M.; Chen, B.; Yin, J.; Jin, H.; Lin, L.; Chen, C.; Zhang, N. Hollow Pd/MOF Nanosphere with Double Shells as Multifunctional Catalyst for Hydrogenation Reaction. *Small*. **2017**, *13*, 1701395.

(34) Zhong, Y.; Mao, Y.; Shi, S.; Wan, M.; Ma, C.; Wang, S.; Chen, C.; Zhao, D.; Zhang, N. Fabrication of Magnetic Pd/MOF Hollow Nanospheres with Double-Shell Structure: Toward Highly Efficient and Recyclable Nanocatalysts for Hydrogenation Reaction. *ACS Appl. Mater. Interfaces*. **2019**, *11*, 32251-32260.

(35) Tang, J.; Salunkhe, R. R.; Liu, J.; Torad, N. L.; Imura, M.; Furukawa, S.; Yamauchi, Y. Thermal Conversion of Core-Shell Metal-Organic Frameworks: A New Method for Selectively Functionalized Nanoporous Hybrid Carbon. *J. Am. Chem. Soc.* **2015**, *137*, 1572-1580.

(36) Kresse, G.; Furthmiiller, J. Efficiency of ab-Initio Total Energy Calculations for Metals and Semiconductors using a Plane-Wave Basis Set. *Comp. Mater. Sci.* **1996**, *6*, 15-50.

(37) Kresse, G.; Furthmuller, Efficient Iterative Schemes for ab Initio Total-Energy Calculations using a Plane-Wave Basis Set. J. *Phys. Rev. B.* **1996**, *54*, 11169-11186.

(38) Perdew, J. P.; Burke, K.; Ernzerhof, M. Generalized Gradient Approximation Made Simple. *Phys. Rev. Lett.* **1996**, *77*, 3865-3868.

(39) Blochl, P. E. Projector Augmented-Wave Method. *Phys. Rev. B.* **1994**, *50*, 17953-17979.

(40) Grimme, S.; Ehrlich, S.; Goerigk, L. Effect of the Damping Function in Dispersion Corrected Density Functional Theory. *J. Comput. Chem.* **2011**, *32*, 1456-1465.

(41) Grimme, S.; Antony, J.; Ehrlich, S.; Krieg, H. A Consistent and Accurate ab Initio Parametrization of Density Functional Dispersion Correction (DFT-D) for the 94 Elements H-Pu. *J. Chem. Phys.* **2010**, *132,*154104.

(42) Guo, C.; Guo, J.; Zhang, Y.; Wang, D.; Zhang, L.; Guo, Y.; Ma, W.; Wang, J. Synthesis of Core-Shell ZIF-67@Co-MOF-74 Catalyst with Controllable Shell Thickness and Enhanced Photocatalytic Activity for Visible Light Driven Water Oxidation. *CrystEngComm*. **2018**, *20*, 7659-7665.

(43) Lin, L.; Zhang, T.; Zhang, X.; Liu, H.; Yeung, K. L.; Qiu, J. New Pd/SiO_2@ZIF-8 Core-Shell Catalyst with Selective, Antipoisoning, and Antileaching Properties for the Hydrogenation of Alkenes. *Ind. Eng. Chem. Res.* **2014**, *53*, 10906-10913.

(44) Rosi, N. L.; Kim, J.; Eddaoudi, M.; Chen, B.; O'Keeffe, M.; Yaghi, O. M. Rod Packings and Metal-Organic Frameworks Constructed from Rod-Shaped Secondary Building Units. *J. Am. Chem. Soc.* **2005**, *127*, 1504-1518.

(45) Chen, G. J.; Ma, H. C.; Xin, W. L.; Li, X. B.; Jin, F. Z.; Wang, J. S.; Liu, M. Y.; Dong, Y. B. Dual Heterogeneous Catalyst Pd-Au@Mn(II)-MOF for One-Pot Tandem Synthesis of Imines from Alcohols and Amines. *Inorg. Chem.* **2017**, *56*, 654-660.

(46) Li, L.; Zhang, N.; Huang, X.; Liu, Y.; Li, Y.; Zhang, G.; Song, L.; He, Hong. Hydrothermal Stability of Core-Shell Pd@$Ce_{0.5}Zr_{0.5}O_2$/Al_2O_3 Catalyst for Automobile Three-Way Reaction. *ACS Catal.* **2018**, *8*, 3222-3231.

(47) Gole, B.; Sanyal, U.; Banerjee, R.; Mukherjee, P. S. High Loading of Pd Nanoparticles by Interior Functionalization of MOFs for Heterogeneous Catalysis. *Inorg. Chem.* **2016**, *55*, 2345-2354.

(48) Tan, K.; Zuluaga, S.; Gong, Q.; Canepa, P.; Wang, H.; Li, J.; Chabal,Y. J.; Thonhauser, T. Water Reaction Mechanism in Metal Organic Frameworks with Coordinatively Unsaturated Metal Ions: MOF-74. *Chem. Mater.* **2014**, *26*, 6886-6895.

(49) Li, H. C.; Liu, W. J.; Han, H. X.; Yu, H. Q. Hydrophilic Swellable Metal-Organic Framework Encapsulated Pd Nanoparticles as an Efficient Catalyst for Cr(VI) Reduction. *J. Mater. Chem. A*. **2016**, *4*, 11680-11687.

(50) Duan, H.; You, R.; Xu, S.; Li, Z.; Qian, K.; Cao, T.; Huang, W.; Bao, X. Pentacoordinated Al^{3+}-Stabilized Active Pd Structures on Al_2O_3-Coated Palladium Catalysts for Methane Combustion. *Angew. Chem. Int. Ed.* **2019**, *58*, 12043-12048.

(51) Lee, A. F.; Naughton, J. N.; Liu, Z.; Wilson, K. High-Pressure XPS of Crotyl Alcohol Selective Oxidation over Metallic and Oxidized Pd(111). *ACS Catal.* **2012**, *2*, 2235-2241.

(52) Guo, C.; Zhang, Y.; Zhang, L.; Guo, Y.; Akram, N.; Wang, J. 2-Methylimidazole-Assisted Synthesis of Nanosized $Cu_3(BTC)_2$ for Controlling the Selectivity of the Catalytic Oxidation of Styrene. *ACS Appl. Nano Mater.* **2018**, *1*, 5289-5296.

(53) Guo, C.; Zhang, Y.; Zhang, L.; Zhang, Y.; Wang, J. 2-Methylimidazole-Assisted Synthesis of a Twodimensional MOF-5 Catalyst with Enhanced Catalytic Activity

for the Knoevenagel Condensation Reaction. *CrystEngComm*. **2018**, *20*, 5327-5331.
(54) Dai, Y.; Gao, X.; Chu, X.; Jiang, C.; Yao, Y.; Guo, Z.; Zhou, C.; Wang, C.; Wang, H.; Yang, Y. On the Role of Water in Selective Hydrogenation of Cinnamaldehyde to Cinnamyl Alcohol on PtFe Catalysts. *J. Catal.*, **2018**, *364*, 192-203.
(55) Liu, J.; Wei, Y.; Li, P.; Zhao, Y.; Zou, R. Selective H_2S/CO_2 Separation by Metal-Organic Frameworks Based on Chemical-Physical Adsorption. *J. Phys. Chem. C*. **2017**, *121*, 13249-13255.
(56) Pei, Y.; Qi, Z.; Goh, T. W.; Wang, L. L.; Maligal-Ganesh, R. V.; MacMurdo, H. L.; Zhang, S.; Xiao, C.; Li, X.; Tao F.; Johnson, D. D.; Huang, W. Intermetallic Structures with Atomic Precision for Selective Hydrogenation of Nitroarenes. *J. Catal.* **2017***, 356,* 307-314.
(57) Mukherjee, S.; Manna, B.; Desai, A. V.; Yin, Y.; Krishna, R.; Babarao, R.; Ghosh, S. K. Harnessing Lewis Acidic Open Metal Sites of Metal-Organic Frameworks: the Foremost Route to Achieve Highly Selective Benzene Sorption over Cyclohexane. *Chem. Commun.* **2016**, *52*, 8215-8218.
(58) Zhang, Z.; Xiao, Y.; Cui, M.; Tang, J.; Fei, Z.; Liu, Q.; Chen, X.; Qiao, X. Modulating the Basicity of Zn-MOF-74 via Cation Exchange with Calcium Ions. *Dalton Trans.* **2019**, *48*, 14971-14974.

TOC Graphic

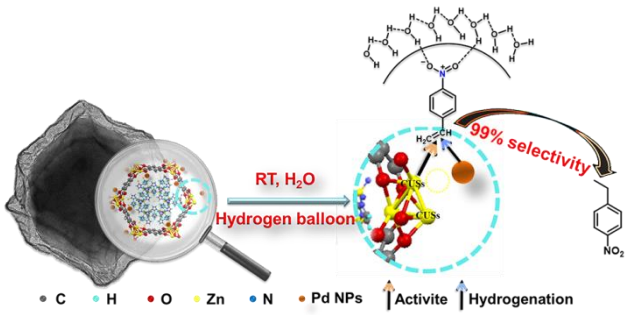
RT, H2O
Hydrogen balloon
99% selectivity
NO2
C
H
O
Zn
N
Pd NPs
Activite
Hydrogenation